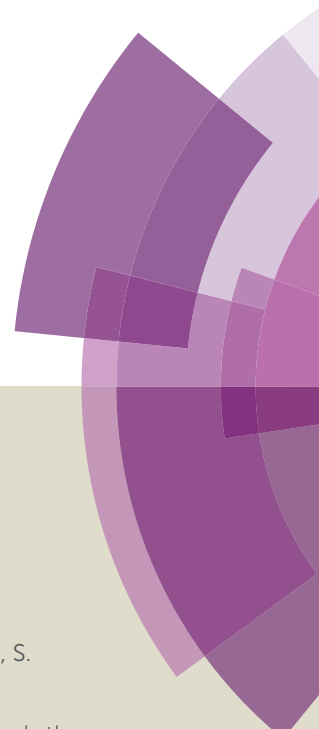


Journal of Materials Chemistry A

Accepted Manuscript



This article can be cited before page numbers have been issued, to do this please use: E. Zhang, Y. Xie, S. Ci, J. Jia, P. Cai, L. Yi and Z. Wen, *J. Mater. Chem. A*, 2016, DOI: 10.1039/C6TA06185K.



This is an *Accepted Manuscript*, which has been through the Royal Society of Chemistry peer review process and has been accepted for publication.

Accepted Manuscripts are published online shortly after acceptance, before technical editing, formatting and proof reading. Using this free service, authors can make their results available to the community, in citable form, before we publish the edited article. We will replace this *Accepted Manuscript* with the edited and formatted *Advance Article* as soon as it is available.

You can find more information about *Accepted Manuscripts* in the [Information for Authors](#).

Please note that technical editing may introduce minor changes to the text and/or graphics, which may alter content. The journal's standard [Terms & Conditions](#) and the [Ethical guidelines](#) still apply. In no event shall the Royal Society of Chemistry be held responsible for any errors or omissions in this *Accepted Manuscript* or any consequences arising from the use of any information it contains.

1 Multifunctional High-activity and Robust Electrocatalyst 2 Derived from Metal-organic Frameworks

3 Erhuan Zhang,^{1,2} Yu Xie,^{1*} Suqin Ci,¹ Jingchun Jia,^{2,3} Pingwei Cai,^{1,2} Luocai Yi,¹
4 Zhenhai Wen^{1,2,3*}

5 *1 Key Laboratory of Jiangxi Province for Persistent Pollutants Control and Resources Recycle,*
6 *Nanchang Hangkong University, Nanchang 330063, P. R. China*

7 *2 Key Laboratory of Design and Assembly of Functional Nanostructures, Fujian Institute of*
8 *Research on the Structure of Matter, Chinese Academy of Sciences, Fuzhou, Fujian 350002, P. R.*
9 *China*

10 *3 Fujian Provincial Key Laboratory of Nanomaterials, Fujian Institute of Research on the*
11 *Structure of Matter, Chinese Academy of Sciences, Fuzhou, Fujian 350002, P. R. China*

12 *E-mail: xieyu_121@163.com, wenzhenhai@fjirsm.ac.cn

13

14 **Abstract:** High-activity electrocatalysts with robust structure are critical for
15 development of renewable-energy technologies. Herein, the hybrid with cobalt
16 nanoparticles embedded in N-doped carbon nanotube (Co@NCNT) was fabricated via
17 economically scalable pyrolysis of mixture of Co-based metal-organic framework
18 (ZIF-67) and dicyandiamide. The as-synthesized Co@NCNT hybrid was
19 characterized by techniques of scanning electron microscope (SEM), transmission
20 electron microscopy (TEM), and X-ray photon spectroscopy (XPS) etc., confirming
21 the Co@NCNT possessed desirable properties of high surface area, robust structure,
22 and good conductivity. Impressively, a series of electrochemical measurements
23 demonstrate the Co@NCNT exhibits high activity and excellent durability toward
24 several important electrochemical reactions, including hydrogen evolution reaction
25 (HER) in pH-universal electrolyte, oxygen reduction reaction (ORR) in both acidic
26 and alkaline media, glucose oxidation reaction (GOR), and oxygen evolution reaction
27 (OER) in alkaline medium, which is mainly benefited from synergistic effects of
28 unique structure, high surface area, and Co nanoparticles and nitrogen dopant in the
29 nanocomposite. Furthermore, a zinc-air battery with the Co@NCNT as cathode

1 material was set up with an outstanding performance, demonstrating its potential
2 application for energy storage and conversion system device.

3

4 **Key words:** Nanohybrids; Cobalt nanoparticles; N-doped carbon; Multifunctional
5 electrocatalyst; Zinc-air battery

6 1. Introduction

7 There has been increasing concerns related to clean and sustainable energy
8 sources due to the depletion of fossil fuel and their deleterious effect on the
9 environment. Lots of electrochemical reactions, such as oxygen reduction reaction
10 (ORR), glucose oxidation reaction (GOR), and overall water splitting, are at the heart
11 of a variety of electrochemical energy conversion and storage system, including
12 metal-air batteries, fuel cell, and water-splitting devices.¹⁻⁴ Given that the catalysts are
13 of great importance to drive these electrochemical reactions, the exploration of new
14 electrocatalyst have been extensively studied in recent years.

15 To date, platinum group metals, due to their high activity, are the dominant
16 electrocatalysts in multidisciplinary fields such as HER,⁵ fuel cells,^{6,7} and sensors.⁸
17 However, the low natural abundance, high cost and easy fading in activity of Pt limit
18 their widespread applications in these systems.⁹ Therefore, it is imperative to develop
19 Pt alternative catalysts with a highly promising family of electrocatalysts. To this end,
20 nanostructured carbon with either loading precious-metal free active substance or
21 doping heteroatom (e.g. N, P, S etc..) have attracted tremendous attention due to their
22 tailorable structures, abundant source, high surface areas, and adjustable chemical
23 composition, which enhance the corresponding catalytic activity for specific
24 electrochemical reactions.¹⁰⁻¹⁶ Among them, transition metal-nitrogen-carbon
25 (Co-N-C) composite have been employed as a competitive electrocatalyst owing to
26 their low cost, excellent activity and good stability, such as Co@NG for ORR/GOR;³
27 Co/CoO@Co-N-C toward ORR, OER and HER;¹⁷ NCNTFs for ORR/OER.¹⁸ The
28 electrocatalytic performance is highly dependent on the structures and morphologies
29 of the carbon support, favorable features with large surface area and high electrical
30 conductivity even make the resultant composites highly competitive to traditional
31 metallic electrocatalysts.¹⁹⁻²¹ Specifically, it is noted that the newly identified Me-N_x

1 (Me = Fe, Co, Ni, Bimetal) sites in the carbon framework are responsible for
2 optimized electrocatalytic activity of the Me,N-doped carbon.²²⁻²⁴ Metal nanoparticles
3 encapsulated by carbon nanotube (Me@CNT) is emerged as a potential catalyst with
4 high structural and chemical durability, as the encasing carbon layers can protect the
5 inner nanoparticles from electrolyte, therefore, exhibit better resistance to corrosion
6 and oxidization from external harsh operating environment as well as avoid the
7 agglomeration with adjacent nanoparticles.²⁵ Also, encapsulation of metallic
8 nanoparticles inside graphitic wall of CNT have been separately confirmed to be able
9 to catalyze water splitting, ORR and sensing.²⁶⁻²⁸ However, the available synthesis
10 procedures for N-doped CNTs usually involve multistep and complicated
11 conditions.^{29, 30}

12 Since metal-organic frameworks (MOFs) were first defined in late 1990s by
13 Yaghi and Li, a rapidly growing development for MOF-based materials has
14 emerged.³¹ In the recent years, MOFs have been developed as sacrificial templates for
15 fabricating MOF-derived carbon (MDC) with heteroatom decoration, long-range
16 ordering, and high porosity via a simple pyrolysis,³² conferring a great opportunity to
17 develop new types of carbon-based nanocomposites as electrode materials for a
18 variety of applications, such as HER,³³ lithium-sulfur battery,³⁴ supercapacitor,³⁵ fuel
19 cell,³⁶ and metal-air batteries.³⁷ Although a number of MOF-derived
20 nanocarbons/metal oxides have been prepared as electrocatalysts, most of them
21 exhibit unsatisfactory electrochemical activity.^{38, 39} Moreover, intermolecular doping
22 into carbon framework with nitrogen can considerably affect the physical properties
23 and thus result in a robust and high-activity catalyst.

24 Up to now, although numerous precious-metal-free nanocatalysts derived from
25 MOFs can be applied in energy storage and conversion systems, it is still highly
26 desirable to design multifunctional electrocatalysts for water splitting, ORR, GOR,
27 and the relevant energy storage devices simultaneously.^{40, 41} Here, we reported our
28 recent efforts in constructing multifunctional electrocatalyst with Co nanoparticles
29 encased in nitrogen-doped CNT, Co@NCNT, which was achieved by one-step and
30 scalable pyrolysis of the mixture of ZIF-67 and dicyandiamide at 750 °C under an
31 inert atmosphere. The ZIF-67 derived Co@NCNT was developed as a robust and

1 highly efficient multifunctional electrocatalyst toward water splitting, ORR, GOR and
2 the promising zinc-air based on its OER/ORR bifunctionality.

3 **2. Experimental section**

4 2.1. Materials

5 Cobalt nitrate hexahydrate ($\text{Co}(\text{NO}_3)_2 \cdot 6\text{H}_2\text{O}$, 99 %), 2-methylimidazole (mIM, 99 %)
6 and KOH were purchased from Shanghai Chemical Reagents, China. Nafion (5 %)
7 and dicyandiamide was obtained from Aladdin. All of the reagents related in this
8 experiment were analytical grade and used without further purification.

9 2.2. Synthesis

10 Synthesis of ZIF-67 crystals: ZIF-67 crystals were synthesized through a
11 room-temperature precipitation. Typically, one solution of $\text{Co}(\text{NO}_3)_2 \cdot 6\text{H}_2\text{O}$ (0.6 g, 2.1
12 mmol) was dissolved in 4 mL DI water, another solution of 2-methylimidazole (7.31 g,
13 89.24 mmol) in a 26 mL DI water was stirred until dissolved instead of methanol
14 solvent. The $\text{Co}(\text{NO}_3)_2$ solution was added to the stirred 2-methylimidazole solution, the
15 liquid immediately turned opaque purple, and then was stirred for 6 h at room
16 temperature (RT). The resulting purple precipitates were collected by centrifugation
17 and washing with ethanol three times and dried in a vacuum at 80 °C for 24 h.⁴² To
18 remove any adsorbed species, the sample was further pretreated by degassing at
19 150 °C for 6 h before all analyses.

20 Synthesis of Co@NCNT: Briefly, Co@NCNT nanocatalyst was synthesized through
21 a solid-phase reaction between ZIF-67 and dicyandiamide. In a typical synthesis, 0.2
22 g of ZIF-67 host and 1.0 g of dicyandiamide were mixed together and ground into a
23 fine powder using a mortar. The mixture was loaded in a ceramic boat and calcined at
24 500 °C for 30 min in a type furnace with a ramping rate of 3 °C /min. We noticed
25 overtly, however, that the optimized heating conditions for devising a cobalt
26 nanoparticles engaged in CNT were thermal-treated under a Ar environment at 500 °C
27 for 30 min, which prevents collapse of the porous structure.⁴³ The parent material
28 placed was further increased to 750 °C at a ramping rate of 1 °C /min and kept at this
29 temperature for 2 h under flowing argon, followed by acid treatment of the resulting

1 material with HCl: HNO₃ = 3:1 (volume ratio) and was stirred for 24 h to remove
2 partial accessible cobalt species to achieve Co@NCNT (etching).⁴⁴ The Co@NCNT
3 prepared at 750 °C was identified as Co@NCNT. Other versions of Co@NCNT
4 prepared at different T_c (i.e., 650, 850 °C) were also investigated.

5 Synthesis of Co@NC: In parallel synthesis, Co@NC was also obtained by direct
6 carbonization of ZIF-67 precursor under the same conditions for comparison, without
7 dicyandiamide in the synthesis.⁴⁵

8 2.3. Characterization

9 The morphology and structure of powder were captured with a transmission electron
10 microscope (TEM, JEM-2010) with an S2 accelerating voltage of 200 kV and a
11 scanning electron microscope (SEM, NOVA NANOSEM450) at an acceleration
12 voltage of 10.0 kV. Power X-ray diffraction (XRD) pattern was collected from a
13 Bruker D8 advance diffractometer using Cu K α radiation ($\lambda = 1.5418 \text{ \AA}$). Specific
14 surface areas, pore volume and pore size distribution of the products were completed
15 from the Brunauer-Emmett-Teller (BET) method using nitrogen adsorption and
16 desorption isotherms on a Micromeritics Instrument Corporation sorption analyzer
17 (Micromeritics TriStar II 3020). X-ray photoelectron spectroscopy (XPS) was
18 conducted by HP 5950A XPS with an Mg K α as source and the C1s peak at 284.6 eV
19 as an internal standard. Electrochemical measurements were carried out on a CHI
20 760E electrochemical analyzer (Shanghai China). A three-electrode system consisting
21 of a glassy carbon (GC) working electrode (3mm in diameter), an Ag/AgCl reference
22 electrode (saturated KCl) and a platinum wire counter electrode, was used.

23 3. Results and discussion

24 There are two main steps involved in the pathway for preparing products. The
25 feasible “one stone two birds” route can endow the final products with two features:
26 (1) metallic Co nanoparticles with electrocatalytic activity, deriving from Co in
27 ZIF-67, are formed through in situ reduction under the presence of the Ar atmosphere,
28 and (2) under the catalytic assistance of Co nanoparticles, one-dimensional (1D)
29 CNTs with N doping are produced with dicyandiamide as carbon and nitrogen source
30 upon its decomposition.^{18, 26, 29, 46-48}

1 Fig. 1a shows scanning electron microscope (SEM) image of ZIF-67 precursor,
2 as expected, ZIF-67 displays a well-defined nanopolyhedron, being well consistent
3 with previous report.^{49, 50} Fig. 1b exhibits a typical SEM image of Co@NCNT, in
4 which one can observe 1D fiber morphology with white dots either at the tip or inside
5 of CNTs. Fig. 1c-d display the transmission electron microscopy (TEM) images,
6 suggesting that the as-prepared Co@NCNT has a number of nanoparticles (NPs) with
7 size around a few nanometers that are dispersed around the carbon nanotube. Fig. 1e
8 shows the high resolution TEM (HRTEM) image, manifesting the carbon shell with a
9 crystal plane spacing of 0.34 nm, corresponding to the (002) diffraction plane of
10 graphite; such core-shell structure enhance the electron transport and suppress the
11 dissolution and agglomeration of NPs.⁵¹ Another HRTEM image also demonstrates
12 nanoparticles are also covered by carbon layers with cobalt nanoparticles as the core
13 and carbon film as the shell, as indicated by the HRTEM image (Fig. 1f). The Co NPs,
14 deriving from reduction of Co ions in ZIF-67 during the pyrolysis process, exhibited
15 the face-centred cubic Co phase. Correspondingly, the cobalt nanoparticles are
16 encapsulated in carbon architecture, which are responsible for catalyzing the growth
17 of carbon nanotubes.^{47, 48} The crystalline cobalt and carbon shells are further proved
18 by the selected area electron diffraction (SAED) pattern (the inset in Fig. 1e).

19 The sample was measured by powder X-ray diffraction (XRD) to characterize
20 the composition and crystalline structure. The XRD profile of as-prepared MOF (Fig.
21 S3a) was in good agreement with the simulated ZIF-67, verifying the formation of
22 pure ZIF-67 crystals. Fig. 2a shows powder X-ray diffraction (XRD) for the
23 Co@NCNT sample. The peaks at 44.4° and 51.7° corresponded to the (111) and (200)
24 planes of Co, suggesting the successful conversion from cobalt ion in ZIF-67 into
25 metallic Co upon heat treatment by mixing ZIF-67 with dicyandiamide. Additionally,
26 the diffraction peak at 26.1° indicated the formation of graphitic carbon during the
27 pyrolysis, being consistent with the presence of CNT, which is coincided with the
28 SAED analysis. Meanwhile, some parallel samples, such as cobalt nanoparticles

1 encapsulated by N-doped carbon (Co@NC) and Co@NCNT after etching, were
2 examined by X-ray diffraction pattern, as revealed in Fig. S3.

3 To get insight into the specific surface area and porous structure of Co@NCNT,
4 N₂ adsorption-desorption and Barret-Joyner-Halenda analysis were further carried out.
5 Fig. 2b displays a typical type IV and an obvious hysteresis loop with a relative
6 pressure ranging from 0.5 to 1.0, suggesting the existence of both micropore and
7 mesopore. Furthermore, a sharp peak is presented at around 2.05 nm in the inset of
8 Fig. 2b, indicating that the porosity of Co@NCNT was dominated by mesopores.
9 According to the testing report, Co@NCNT possesses a specific surface area of 97.4
10 m² g⁻¹, lower than that of ZIF-67 precursor (Fig. S4).

11 The chemical composition and nitrogen bonding configuration in Co@NCNT
12 were characterized by X-ray photon spectroscopy (XPS). Fig. 3a presents the XPS
13 spectrum of Co@NCNT with characteristic peaks of C1s (285.1), N1s (400.1 eV),
14 adventitious O 1s (531.6 eV) and Co 2p (781.3 eV). The high-resolution XPS spectra
15 of N 1s and Co 2p were further analyzed. Fig. 3b is the complex N 1s spectra, which
16 can be deconvoluted into five peaks, corresponding to five different types of N atom:
17 pyridine-type N (398.4 eV), Co-N_x (399.3 eV), pyrrole-type N (400.8 eV),
18 graphite-type N (401.2 eV), and oxidized N (404.5 eV). Of these types of N,
19 pyridine-type N and graphite-type N have been demonstrated to be the active sites
20 toward ORR.^{52, 53} After deconvolution, the complex Co 2p spectrum (Fig. 3c)
21 suggests the existence of four chemically distinct phases: metallic Co (778.5 eV),
22 Co³⁺ (779.5 eV), Co²⁺ (780.5 eV) and Co-N_x (782.5 eV), whereas oxidized Co may
23 be induced from oxidation of partial cobalt nanoparticles. Interestingly, the content of
24 N in Co@NCNT (3.08 %) is higher than that in Co@NC (2.38 %) according to the
25 elemental analysis result, we can presume that the existence of graphic CNT is helpful
26 to improve the N-doping in the obtained nanostructure (Table S1).

27 The polarization curves of the samples (Co@NCNT prepared at different
28 temperatures 650 °C, 750 °C, 850 °C) in 0.5 M H₂SO₄ with a scan rate of 5 mV s⁻¹
29 are illustrated in Fig. S5. Specially, Co@NCNT-750 exhibits the best catalytic
30 activity with a small onset overpotential of about 104 mV (the overpotential that the
31 electrocatalyst requires to yield a current density of 1 mA cm⁻²) and an overpotential

1 of ca. 210 mV at 10 mA cm⁻² versus the reversible hydrogen electrode (RHE). Then,
2 the electrocatalytic activity toward HER in pH-universal electrolyte was measured by
3 a glassy carbon electrode (GCE) modified with Co@NCNT formed at 750 °C as the
4 working electrode. For comparison, the commercial Pt/C (20 % loading) and Co@NC
5 were examined under the identical condition. Fig. 4a shows the linear sweep
6 voltammograms (LSV) curve of Co@NCNT in 0.5 M H₂SO₄ with a scan rate of 5 mV
7 s⁻¹. The Co@NCNT yields a current density of 1 mA cm⁻² at an overpotential of
8 around 0.105 V versus RHE; this value is quite close to the thermodynamic potential
9 of HER (i.e., 0 V). Moreover, the Co@NCNT affords a current density of 10 mA cm⁻²
10 at a small overpotential (η) of 0.21 V, which is smaller than that of Co@NC (10 mA
11 cm⁻², 0.32 V). These results suggest the Co@NCNT electrocatalyst required a rather
12 lower overpotential to yield a current densities at 1 mA cm⁻² and 10 mA cm⁻²
13 compared with Co@NC, may resulting from CNT channels which could yield easier
14 mass transportation, the more amount of nitrogen dopant resulting in CoN_x sites in
15 hybrids.^{23, 54}

16 We carried out the further analysis of the corresponding Tafel plots to study the
17 kinetics of HER processes. Fig. 4b displays Tafel plots for Pt/C, Co@NCNT and
18 Co@NC, respectively. The Tafel plot value for Pt/C is about 30 mV dec⁻¹, which is
19 consistent with literature values.⁵⁵ For Co@NCNT, the value is calculated to be ~93
20 mV dec⁻¹ in the region of η = 80-150 mV versus reversible hydrogen electrode (RHE),
21 which exhibits much lower Tafel slope than that of the Co@NC (248 mV dec⁻¹).
22 Catalytic stability is of paramount importance for an electrocatalyst because HER
23 catalysis mostly works in an extreme condition of strong acid or alkaline media. To
24 verify it, time-dependent current density is conducted to characterize the
25 electrocatalytic stability of the sample in 0.5 M H₂SO₄. The Co@NCNT electrode
26 presents a nearly unchanged current density over a period of 20000 s at an applied
27 potential of -0.3 V (Fig. S7a), which is attributed to the protected Co⁰ embedded in
28 CNT in acid environment. We also probe the electrocatalytic activity of Co@NCNT
29 for HER in alkaline and neutral media. As seen from Fig. 4c, the Co@NCNT shows
30 high catalytic activity toward HER in 0.1 M KOH solution. Also, compared to the
31 Co@NC, the Co@NCNT has a more decent electrocatalytic activity toward HER in
32 neutral solution (pH = 7), as evidenced by its more positive onset potential and

1 current density Fig. 4d. The Tafel curves and catalytic stabilities were also
2 investigated in pH-universal solutions (Fig. S6 and S7), further confirming that the
3 Co@NCNT electrocatalyst perform well as a promising HER electrocatalyst in
4 pH-universal electrolyte (Table S2).

5 In order to better understand the formation mechanism, ZIF-67 and
6 dicyandiamide were pyrolyzed at different temperatures (650 °C, 750 °C, 850 °C).
7 The catalytic activity toward ORR for the corresponding materials were investigated
8 in alkaline electrolyte. Among all the catalysts, the material derived at 750 °C exhibits
9 the most positive onset potential and the highest limiting current density of 6.41 mA
10 cm⁻² in Fig. S8. To further confirm the ORR catalytic activities of the Co@NCNT-750,
11 cyclic voltammetry (CV) is first tested in basic solution at a scan rate of 50 mV s⁻¹. As
12 depicted in Fig. S11a, there is a well-defined cathodic peak with current density of
13 3.49 mA cm⁻² at 0.814 V (vs. RHE) for the Co@NCNT in O₂-saturated 0.1 M KOH,
14 whereas such a peak is absent in Ar-saturated aforementioned solution. The catalytic
15 activity toward ORR for the Co@NCNT approaches the level for the commercial Pt/C
16 in alkaline electrolyte (Fig. S7b). The ORR polarization curves of Co@NCNT,
17 Co@NC and the Pt-C in alkaline media are shown in Fig. 5a. The onset potential with
18 0.1 mA cm⁻² and the half-wave potential (E_{1/2}) of Co@NCNT catalyst at 1600 rpm are
19 1.03 V and 0.828 V, respectively. Both values are higher than those of Co@NC
20 (0.946 V, 0.812V) and are comparable to commercial Pt/C (0.97 V, 0.85 V).
21 N-doping has been known to produce defects in CNTs, resulting in the formation of
22 O₂ adsorption sites, are believed to be an important contributing factor to high activity
23 of carbon-based catalysts. Since there is more N-doping in NCNT than that of
24 Co@NC, it is thus reasonable to conclude that the N-doping in CNT is crucial for
25 enhancing ORR electrocatalytic activity. The Tafel plot can be derived from the
26 polarization curve (Fig. S13a), which is 94.8 mV dec⁻¹ at low overpotential, close to
27 the 92.53 mV dec⁻¹ of the Pt/C, indicating that Co@NCNT possesses a faster electron
28 transfer rate and highly efficient reactant diffusion for ORR. In order to better
29 elucidate the role of metallic cobalt for ORR, the as-synthesized Co@NCNT is etched
30 using acid as control experiment. Interestingly, the Co@NCNT shows much more
31 excellent activity for ORR than the Co@NCNT after etching (less cobalt loading),

1 indicating metallic cobalt encapsulated in CNT do contribute to improving ORR
2 performance.

3 To investigate the electron-transfer mechanism upon catalyzing ORR in 0.1 M
4 KOH, the relative kinetic parameters were analyzed using Koutecky-Levich (K-L)
5 equations at various rotating speeds. Fig. 5b shows a set of plots of the inverse current
6 density J^{-1} versus $\omega^{-1/2}$, in which the intercept corresponds to J_K and the slope
7 reflecting so-called B on the basis of Koutecky-Levich equation (Equation 1,
8 Supporting information). The electron transfer number (n) for Co@NCNT is
9 calculated to be 3.90 for ORR, suggesting 4-electron pathway to H₂O upon ORR
10 catalytic process. To further validate the ORR catalytic pathways of the hybrid
11 materials, we performed rotating ring-disk electrode (RRDE) technique. The peroxide
12 yield and electron transfer number (Fig. 5d), can be calculated based on Equations (3)
13 and (4) (Supporting information). Specially, the Pt ring was polarized at 1.5 V (vs.
14 RHE) in alkaline electrolyte. A high n (3.95-3.99) for Co@NCNT, calculated from
15 RRDE, is consistent with the result obtained from the Koutecky-Levich plots on the
16 basis of RDE measurements, reconfirming the ORR catalyzed by Co@NCNT is
17 dominated by 4e reduction. While the Co@NC shows a lower electron-transfer
18 number (n) of 3.61-3.86 based on testing results of RRDE.

19 Besides the high activity, the catalyst also exhibits methanol tolerance and
20 excellent stability. Almost no variation in the LSV curve for Co@NCNT can be
21 observed upon the addition of methanol to electrolyte, while the ORR current of Pt/C
22 shifted from a cathodic current to a reversed anodic current in a very short time due to
23 methanol oxidation reaction (Fig. 5e).⁵⁶ The results exemplify that Co@NCNT has
24 strong immunity toward methanol crossover effect. Therefore, the remarkably
25 improved stability and methanol tolerance of Co@NCNT made it a feasible candidate
26 for ORR, especially for direct methanol fuel cells. Additionally, the catalytic stability
27 of Co@NCNT for ORR was evaluated using chronoamperometric measurement.
28 Moreover, almost 80 % of the initial current remain at the Co@NCNT electrode after
29 10000 s, whereas Pt/C only retains 60 % of its initial current, indicating that the
30 hybrid exhibits superior durability to Pt/C catalyst in 0.1 M KOH (Fig. 5f). It should
31 be noted that the Co@NC initially exhibits a drastic decrease in the current density
32 and then remains a good stability.

1 Furthermore, the Co@NCNT catalyst was also found to be active for ORR in
2 acidic (Fig. S14b). The ORR peak at 0.60 V (*vs.* RHE) suggests a good catalytic
3 activity for Co@NCNT in O₂ saturated 0.5 M H₂SO₄. The E_{1/2} and the
4 diffusion-limited current density (J_L) are 0.605 V and 4.61 mA cm⁻², respectively;
5 these performance value are very comparable to commercial Pt/C electrocatalyst, but
6 are superior to those of Co@NCNT (etching) (0.525 V and 4.32 mA cm⁻²) and
7 Co@NC (0.418 V and 2.19 mA cm⁻²). We conducted the rotating-disk electrode
8 (RDE) measurements at different rotation rates to assess the ORR kinetics of
9 Co@NCNT in acidic electrolyte (Fig. S10c). The Co@NCNT hybrid exhibits good
10 linearity with near parallelism of the fitting lines, suggesting first-order reaction
11 kinetics toward the concentration of dissolved oxygen. Based on the Koutecky-Levich
12 equation, the electron transfer number of Co@NCNT hybrid is approximately 3.4,
13 suggesting a favorable four-electron pathway for ORR. To further evaluate the ORR
14 pathway for the Co@NCNT, the ORR test was assessed in acidic solution with RRDE
15 measurement (Fig. S15a). The measured H₂O₂ yields are below 42 % in acidic
16 solution, corresponding with an electron transfer number of 3.16-3.86 (Fig. S15c,
17 Table S4). The stability and possible crossover effects of the catalysts are also two
18 major challenge for evaluation of their practical application in acid fuel cells. The
19 Co@NCNT shows excellent long-term stability (Fig. S14d) and tolerance to methanol
20 poisoning effects (Fig S16a), which made it promising for ORR and other reactions in
21 acid media. In this system, direct contact of Co nanoparticles with harsh environments
22 such as acid medium, oxygen, is avoided. However, the chainmail for catalyst does
23 not impede the activation of O₂ and the catalyst also has a rather high activity and
24 long-living stability.⁵⁷

25 We further investigated the electrochemical catalytic properties of the
26 Co@NCNT hybrid by studying its electrochemical response to glucose. The CVs of
27 the Co@NCNT and Co@NC modified glass carbon electrode (GCE) were
28 investigated in alkaline solution (0.1 M KOH) within the scope change of potential
29 from 0.86 V to 1.56 V (*vs.* RHE) at a scan rate of 50 mV/s (Fig. 6a). Without glucose
30 addition, the CV curve of the Co@NCNT in the electrolyte (0.1 M KOH) suggest a
31 pair of well-defined redox peaks observed with the anodic peak at around 1.31 V and
32 the cathodic peak at around 1.05 V (*vs.* RHE), which can be attributed to the

1 oxidation of metallic cobalt and reduction of high valence of Co compound,
2 respectively. After the injection of glucose (concentration of glucose in alkaline
3 solution is 3.0 mM), the Co@NCNT shows a significant higher current increase at the
4 anodic peak than the Co@NC electrode, suggesting the Co@NCNT exhibits a better
5 catalytic activity toward GOR. In order to study the effect of scan rate on glucose
6 oxidation at the Co@NCNT electrode in 0.1 M KOH, the dependence of peak
7 currents on different scan rates in the range from 20-100 (mV s^{-1}) was plotted (Fig.
8 S17a). The anodic peak shows a positive shift and the cathodic peak moves negatively
9 with the increase the scanning rates, indicating a quasi-reversible electron transfer
10 process based on the electrochemical reaction. The peak current densities for both
11 oxidation and reduction are proportional to square root of scan rate (Fig. S17b), which
12 suggests that the redox reaction is a typical diffusion-controlled electrochemical
13 process. The sensing performance of Co@NCNT is investigated at different potentials
14 versus time with the successive addition of 0.2 mM glucose. A current increase is
15 observed with per addition of glucose at applied potentials are 1.314 V, 1.364 V, and
16 1.414 V, respectively (Fig. S18). Considering that a relatively low potential of glucose
17 detection is of great benefit to reduce the background current and interference, 1.364
18 V is selected as the optimal working potential for amperometric detection of glucose
19 in the subsequent studies.

20 The typical amperometric responses of Co@NCNT/GCE are examined by the
21 successive step-wise addition of different amount of glucose in the 0.1 M KOH
22 solution stirred constantly at 1.364 V. As expected, the Co@NCNT electrode shows a
23 steep increase in current response to the addition of glucose concentration (Fig. 6b),
24 and a steady-state current achieved within 3s, indicating that the Co@NCNT exhibits
25 sensitive and rapid response to glucose oxidation reaction. The calibration curve
26 based on the amperometric results is plotted (Fig. 6c), which shows a linear current
27 response over the glucose concentration in the range of 0.005-0.395 mM with a
28 sensitivity of $732.14 \text{ uA mM}^{-1} \text{ cm}^{-1}$ and a correlation coefficient of 0.998.
29 Furthermore, the detection limit of Co@NCNT can reach 0.33 μM basing on a
30 signal-to-noise ratio of 3 (S/N), manifesting a high sensitivity of the Co@NCNT
31 electrode sensor (Table S5). The selectivity of the Co@NCNT for glucose detection is
32 evaluated against the normal co-existed interfering species in human blood, such as

1 dopamine (DA), ascorbic acid (AA), and uric acid (UA). Fig. 6d shows the
2 amperometric response of the Co@NCNT modified electrode in electrolyte
3 containing 1.0 mM glucose, DA (0.1 mM), AA (0.1 mM) and UA (0.1 mM). At an
4 applied potential of 1.364 V, the electrochemical responses of these interfering
5 species are almost negligible comparing with that of glucose at the Co@NCNT
6 electrode, suggesting a good selective detection of glucose. The successive addition of
7 lactose, maltose, mannose, sucrose, fructose with the same concentration is also
8 investigated to demonstrate that the physiological level of saccharides will not affect
9 the detection of glucose (Fig. S19). Additionally, the reproducibility and stability of
10 the Co@NCNT electrode for glucose are also investigated. The relative standard
11 deviation (R.S.D.) of 3.76 % (n = 8) for 0.2 mM glucose demonstrated a good
12 reproducibility of the as-obtained Co@NCNT biosensor.

13 In our study, the Co@NCNT hybrid also showed excellent catalytic activity for
14 the water-oxidation reaction in 1.0 M KOH with a scan rate of 5 mV s⁻¹. The
15 polarization curve of Co@NC reveals an overpotential of 461 mV to reach current
16 density of 10 mA cm⁻² (Fig. 7a). With the presence of N-doped CNT, Co@NCNT
17 with feasible channel need overpotential of 429 mV to achieve current density of 10
18 mA cm⁻², whereas a higher overpotential of 488 mV is required for the Pt/C catalyst.
19 To further study the OER activity, Fig. 7b clearly showed the Tafel plots which are
20 derived from polarization curves by Tafel equation. The enhanced catalytic activity of
21 the Co@NCNT is also reflected by its low Tafel slope of 116 mV dec⁻¹, which is
22 much smaller than that of Pt/C (183 mV dec⁻¹) (Fig. 7b). Moreover, the smaller Tafel
23 slope indicates a more convenient charge transfer within the interface between
24 Co@NCNT and electrolyte.

25 Rechargeable zinc-air batteries often require a bifunctional electrocatalyst toward
26 ORR and OER at the cathode side. We therefore set up a homemade zinc-air battery
27 with the Co@NCNT as the air cathode and Zn foil as the anode (Fig. 7c). The zinc-air
28 battery delivers an open circuit voltages of ~1.5 V. Fig. 7d shows the polarization
29 curves and the corresponding power density plots of the three sets of zinc-air batteries.
30 The zinc-air battery with Co@NCNT as air cathode shows a current densities of 73.10

1 mA cm⁻² at a voltage of 0.8 V, a much higher current density than that for the zinc-air
2 battery with Co@NC as air cathode (59.02 mA cm⁻²). In addition, the maximum
3 power density of Co@NCNT is close to 138.82 mW cm⁻²; this value is comparable to
4 that of Pt/C system (136.25 mW cm⁻²). Both current density and power density values
5 for Co@NCNT compare favorably to the most reported values for the earlier primary
6 batteries.^{58, 59} The cycling stability of the Zn-air battery was further studied through
7 galvanostatically charging and discharging at a current density of 10 mA cm⁻² with
8 the 10 min cycling period for 16 h. Compared with Pt/C-based battery, the
9 Co@NCNT manifests a smaller discharge-charge voltage gap and a less activity
10 decay (Fig. 7e). These results demonstrated that the zinc-air cell with Co@NCNT as
11 air cathode can be afforded by its excellent activity and good stability for battery
12 application.

13 Considering the aforementioned results, coupled with the recent theoretical
14 calculations on metal/nitrogen doped CNTs, the enhanced electrocatalytic activity of
15 Co@NCNT towards HER, ORR, GOR and OER is probably owing to the following
16 synergistic catalytic effects between the N dopants and carbon-coated Co
17 nanoparticles in Co@NCNTs: (1) the improved N doping level into carbon
18 nanomaterials results in electron modulation with changing the charge distribution
19 and electronic properties; In addition, the formation of pyridine-type N and
20 graphite-type N and Co-N_x species in Co@NCNT probably lead to a synergistic
21 catalytic effect to promote the electrocatalytic activity; Moreover, more active sites,
22 such as, topological defects, and edge effects, could further promote the catalytic
23 activity. (2) The incorporation of the one-dimensional CNT is favorable to prepare the
24 three dimensional interpenetrated network structure, further lowering the internal
25 resistance, enhancing the structural stability, and providing convenient channel for the
26 electron transport. (3) Co/CoN_x, as active species, is helpful for the formation of
27 CNTs. The interaction of Co NPs with the graphitic walls of CNTs may decrease their
28 local work function, as a result of electron transfer from Co to CNTs. Additionally,
29 the geometric confinement of Co/CoN_x inside CNTs can significantly improve the

1 catalytic activity (e.g HER, ORR, GOR and OER). Nevertheless, all these possible
2 scenarios still call for further in-depth mechanistic investigation.

3 **4. Conclusion**

4 In summary, we have developed a facile strategy for the synthesis of Co@NCNT
5 with cobalt nanoparticles embedded in N-doped carbon nanotube, which was then
6 studied as a multifunctional catalyst for electrochemical water splitting, ORR, and
7 GOR. The Co@NCNT composites show advantages of low-cost, high efficient, and
8 good stability in electrocatalysis. Electrochemical measurements confirm that the
9 introduction of nitrogen into metal/carbon composites play an important role on the
10 improved electrocatalytic performance. The attractive properties suggest that the
11 Co@NCNT can be developed as a promising Pt-alternative catalyst in
12 electrochemical renewable energies technologies.

14 **Acknowledgements**

15 This work was supported by the National Natural Science Foundation of China
16 (21566025 and 51273089) and the Natural Science Foundation of Jiangxi Province
17 (20152ACB21019 and 20132BAB203018).

18 **References:**

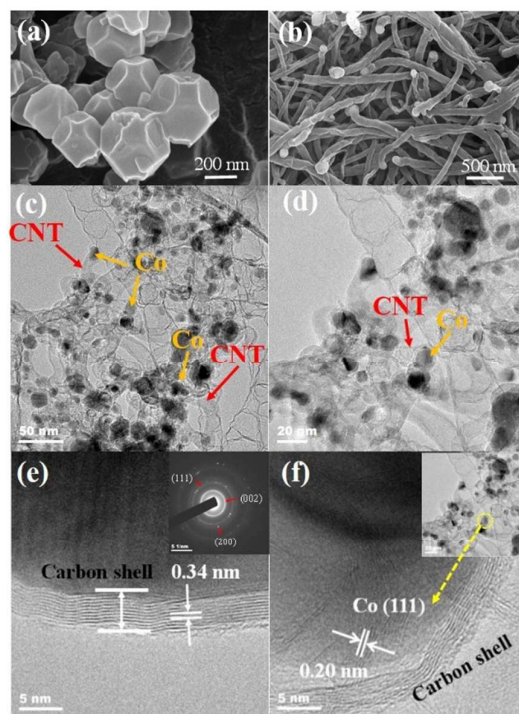
- 19 [1] J. S. Lee, S. Tai Kim, R. Cao, N. S. Choi, M. Liu, K. T. Lee and J. Cho, *Adv.*
20 *Energy Mater.*, 2011, **1**, 34-50.
21 [2] R. Bashyam, P. Zelenay, *Nature*, 2006, 443, 63-66.
22 [3] S. Ci, Z. Wen, S. Mao, Y. Hou, S. Cui, Z. He, J. Chen, *Chem. Commun.*, 2015, 51,
23 9354-9357.
24 [4] C.G. Morales-Guio, L.-A. Stern, X. Hu, *Chem. Soc. Rev.*, 2014, 43, 6555-6569.
25 [5] S. Bai, C. Wang, M. Deng, M. Gong, Y. Bai, J. Jiang, Y. Xiong, *Angew. Chem. Int.*
26 *ed.*, 2014, 53, 12120-12124.

- 1 [6] Y. Bing, H. Liu, L. Zhang, D. Ghosh, J. Zhang, *Chem. Soc. Rev.*, 2010, 39,
2 2184-2202.
- 3 [7] Z. Wen, J. Liu, J. Li, *Adv. Mater.*, 2008, 20, 743-747.
- 4 [8] D. Zhai, B. Liu, Y. Shi, L. Pan, Y. Wang, W. Li, R. Zhang, G. Yu, *ACS Nano*, 7,
5 2013, 3540-3546.
- 6 [9] Y.J. Tang, M.R. Gao, C.H. Liu, S.L. Li, H.L. Jiang, Y.Q. Lan, M. Han, S.H. Yu,
7 *Angew. Chem. Int. ed.*, 2015, 54, 12928-12932.
- 8 [10] L. Zhao, R. He, K.T. Rim, T. Schiros, K.S. Kim, H. Zhou, C. Gutiérrez, S.
9 Chockalingam, C.J. Arguello, L. Pálová, *Science*, 2011, 333, 999-1003.
- 10 [11] Y. Jiao, Y. Zheng, M. Jaroniec, S.Z. Qiao, *J. Am. Chem. Soc.*, 2014, 136,
11 4394-4403.
- 12 [12] Z. Wen, S. Ci, Y. Hou, J. Chen, *Angew. Chem. Int. ed.*, 2014, 53, 6496-6500.
- 13 [13] M. Shalom, S. Gimenez, F. Schipper, I. Herraiz-Cardona, J. Bisquert, M.
14 Antonietti, *Angew. Chem. Int. ed.*, 2014, 126, 3728-3732.
- 15 [14] Y. Zheng, Y. Jiao, Y. Zhu, L.H. Li, Y. Han, Y. Chen, A. Du, M. Jaroniec, S.Z.
16 Qiao, *Nat. Commun.*, 2014, 5.
- 17 [15] Y. Hou, H. Yuan, Z. Wen, S. Cui, X. Guo, Z. He, J. Chen, *J. Power Sources*,
18 2016, 307, 561-568.
- 19 [16] G. Srinivas, T. Zhao, S.A. Shevlin, Z.X. Guo, *Energy Environ. Sci.*, 2016, 9,
20 1661-1667.
- 21 [17] X. Zhang, R. Liu, Y. Zang, G. Liu, G. Wang, Y. Zhang, H. Zhang and H. Zhao,
22 *Chem. Commun.*, 2016, 52, 5946-5949.
- 23 [18] B. Y. Xia, Y. Yan, N. Li, H. B. Wu, X. W. Lou and X. Wang, *Nature Energy*,
24 2016, 1, 15006-15013.
- 25 [19] G. Wu, K. L. More, C. M. Johnston and P. Zelenay, *Science*, 2011, 332, 443-447.
- 26 [20] Y. Wu, M. Chen, Y. Han, H. Luo, X. Su, M.-T. Zhang, X. Lin, J. Sun, L. Wang,
27 L. Deng, W. Zhang, R. Cao, *Angew. Chem. Int. ed.*, 2015, 54, 4870-4875.
- 28 [21] J. Liang, R. F. Zhou, X. M. Chen, Y. H. Tang, S. Z. Qiao, *Adv. Mater.*, 2014,
29 26, 6074-6079.
- 30 [22] H.-W. Liang, S. Brüller, R. Dong, J. Zhang, X. Feng and K. Müllen, *Nature*
31 *commun.*, 2015, 6.
- 32 [23] B. Bayatsarmadi, Y. Zheng, Y. Tang, M. Jaroniec and S. Z. Qiao, *Small*, 2016,
33 12, 3703-3711.

- 1 [24] J. Wei, Y. Hu, Z. Wu, Y. Liang, S. Leong, B. Kong, X. Zhang, D. Zhao, G. P.
2 Simon and H. Wang, *J. Mater. Chem. A*, 2015, **3**, 16867-16873.
- 3 [25] H. Zhang, Z. Ma, J. Duan, H. Liu, G. Liu, T. Wang, K. Chang, M. Li, L. Shi, X.
4 Meng, K. Wu and J. Ye, *ACS nano*, 2015, **10**, 684-694.
- 5 [26] D. Deng, L. Yu, X. Chen, G. Wang, L. Jin, X. Pan, J. Deng, G. Sun, X. Bao,
6 *Angew. Chem. Int. ed.*, 2013, **52**, 371-375.
- 7 [27] C. Soldano, *Prog Mater Sci.*, 2015, **69**, 183-212.
- 8 [28] Z. Wen, S. Ci, Y. Hou, J. Chen, *Angew. Chem. Int. ed.*, 2014, **53**, 6496-6500.
- 9 [29] P. Su, H. Xiao, J. Zhao, Y. Yao, Z. Shao, C. Li, Q. Yang, *Chem. Sci.*, 2013, **4**,
10 2941-2946.
- 11 [30] Y. Fang, X. Li, F. Li, X. Lin, M. Tian, X. Long, X. An, Y. Fu, J. Jin, J. Ma, *J.*
12 *Power Sources*, 2016, **326**, 50-59.
- 13 [31] H. Li, M. Eddaoudi, M. O'Keeffe, O.M. Yaghi, *Nature*, 1999, **402**, 276-279.
- 14 [32] J.-K. Sun, Q. Xu, *Energy Environ. Sci.*, 2014, **7**, 2071-2100.
- 15 [33] Y. Hou, Z. Wen, S. Cui, S. Ci, S. Mao, J. Chen, *Adv. Funct. Mater.*, 2015, **25**,
16 872-882.
- 17 [34] H.B. Wu, S. Wei, L. Zhang, R. Xu, H.H. Hng, X.W.D. Lou, *Chemistry-A*
18 *European Journal*, 2013, **19**, 10804-10808.
- 19 [35] B. Liu, H. Shioyama, T. Akita, Q. Xu, *J. Am. Chem. Soc.*, 2008, **130**, 5390-5391.
- 20 [36] S. You, X. Gong, W. Wang, D. Qi, X. Wang, X. Chen, N. Ren, *Adv. Energy*
21 *Mater.*, 2016, **6**.
- 22 [37] Y. Liang, H. Wang, J. Zhou, Y. Li, J. Wang, T. Regier, H. Dai, *J. Am. Chem.*
23 *Soc.*, 2012, **134**, 3517-3523.
- 24 [38] D. Zhao, J.-L. Shui, L. R. Grabstanowicz, C. Chen, S. M. Commet, T. Xu, J. Lu
25 and D.-J. Liu, *Adv. Mater.*, 2014, **26**, 1093-1097.
- 26 [39] Z.-S. Wu, L. Chen, J. Liu, K. Parvez, H. Liang, J. Shu, H. Sachdev, R. Graf, X.
27 Feng and K. Müllen, *Adv. Mater.*, 2014, **26**, 1450-1455.
- 28 [40] J. Song, C. Zhu, S. Fu, Y. Song, D. Du and Y. Lin, *J. Mater. Chem. A*, 2016, **4**,
29 4864-4870.
- 30 [41] X. Li, Y. Fang, S. Zhao, J. Wu, F. Li, M. Tian, X. Long, J. Jin and J. Ma, *J.*
31 *Mater. Chem. A*, 2015, **3**, 17392-17402.
- 32 [42] J. Qian, F. Sun, L. Qin, *Mater Lett.*, 2012, **82**, 220-223.

- 1 [43] R.R. Salunkhe, J. Tang, Y. Kamachi, T. Nakato, J.H. Kim, Y. Yamauchi, *ACS*
2 *Nano*, 2015, 9, 6288-6296.
- 3 [44] W. Xia, J. Zhu, W. Guo, L. An, D. Xia, R. Zou, *J. Mater. Chem. A*, 2014, 2,
4 11606-11613.
- 5 [45] Y. Hou, J. Li, Z. Wen, S. Cui, C. Yuan, J. Chen, *Nano Energy*, 2015, 12, 1-8.
- 6 [46] A. Fischer, J.O. Müller, M. Antonietti, A. Thomas, *ACS Nano*, 2008, 2,
7 2489-2496.
- 8 [47] H. T. Chung, J. H. Won and P. Zelenay, *Nat. Commun.*, 2013, 4, 1922-1926.
- 9 [48] Q. Li, P. Xu, W. Gao, S. Ma, G. Zhang, R. Cao, J. Cho, H.L. Wang, G. Wu, *Adv.*
10 *Mater.*, 2014, 26, 1378-1386.
- 11 [49] S. Yang, L. Peng, P. Huang, X. Wang, Y. Sun, C. Cao, W. Song, *Angew. Chem.*
12 *Int. ed.*, 2016, 128, 4084-4088.
- 13 [50] Y.Z. Chen, C. Wang, Z.Y. Wu, Y. Xiong, Q. Xu, S.H. Yu, H.L. Jiang, *Adv.*
14 *Mater.*, 2015, 27, 5010-5016.
- 15 [51] J. Deng, P. Ren, D. Deng, L. Yu, F. Yang, X. Bao, *Energy Environ. Sci.*, 2014, 7
16 1919-1923.
- 17 [52] D. Guo, R. Shibuya, C. Akiba, S. Saji, T. Kondo, J. Nakamura, *Science*, 2016,
18 351, 361-365.
- 19 [53] Z. Li, M. Shao, L. Zhou, Q. Yang, C. Zhang, M. Wei, D.G. Evans, X. Duan,
20 *Nano Energy*, 2016, 25, 100-109.
- 21 [54] J. Deng, P. Ren, D. Deng, X. Bao, *Angew. Chem. Int. ed.*, 2015, 54, 2100-2104.
- 22 [55] E.J. Popczun, J.R. McKone, C.G. Read, A.J. Biech, A.M. Wiltrout, N.S. Lewis,
23 R.E. Schaak, *J. Am. Chem. Soc.*, 2013, 135, 9267-9270.
- 24 [56] Y. Zheng, Y. Jiao, J. Chen, J. Liu, J. Liang, A. Du, W. Zhang, Z. Zhu, S.C. Smith,
25 M. Jaroniec, *J. Am. Chem. Soc.*, 2011, 133, 20116-20119.
- 26 [57] X. Cui, P. Ren, D. Deng, J. Deng, X. Bao, *Energy Environ. Sci.*, 2016, 9,
27 123-129.
- 28 [58] J. Zhang, Z. Zhao, Z. Xia, L. Dai, *Nat. Nanotechnol.*, 2015, 10, 444-452.
- 29 [59] M.G. Park, D.U. Lee, M.H. Seo, Z.P. Cano, Z. Chen, *Small*, 2016, 12,
30 2707-2714.
- 31
32

1

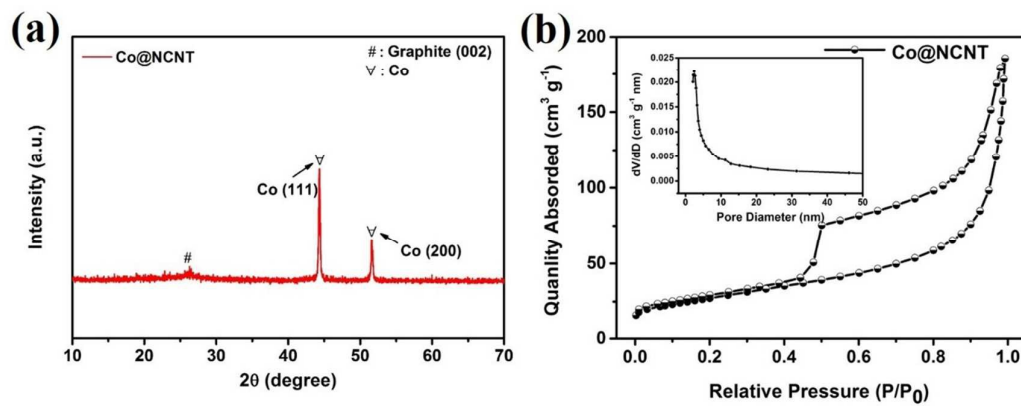


1

2 **Fig. 1.** SEM images of ZIF-67 (a) and Co@NCNT (b). TEM images of Co@NCNT (c,
3 d), HRTEM images of Co@NCNT (e, f), the inset in (e) showing the SAED of the
4 Co@NCNT and the inset in (f) showing the Fig. d.

5

6

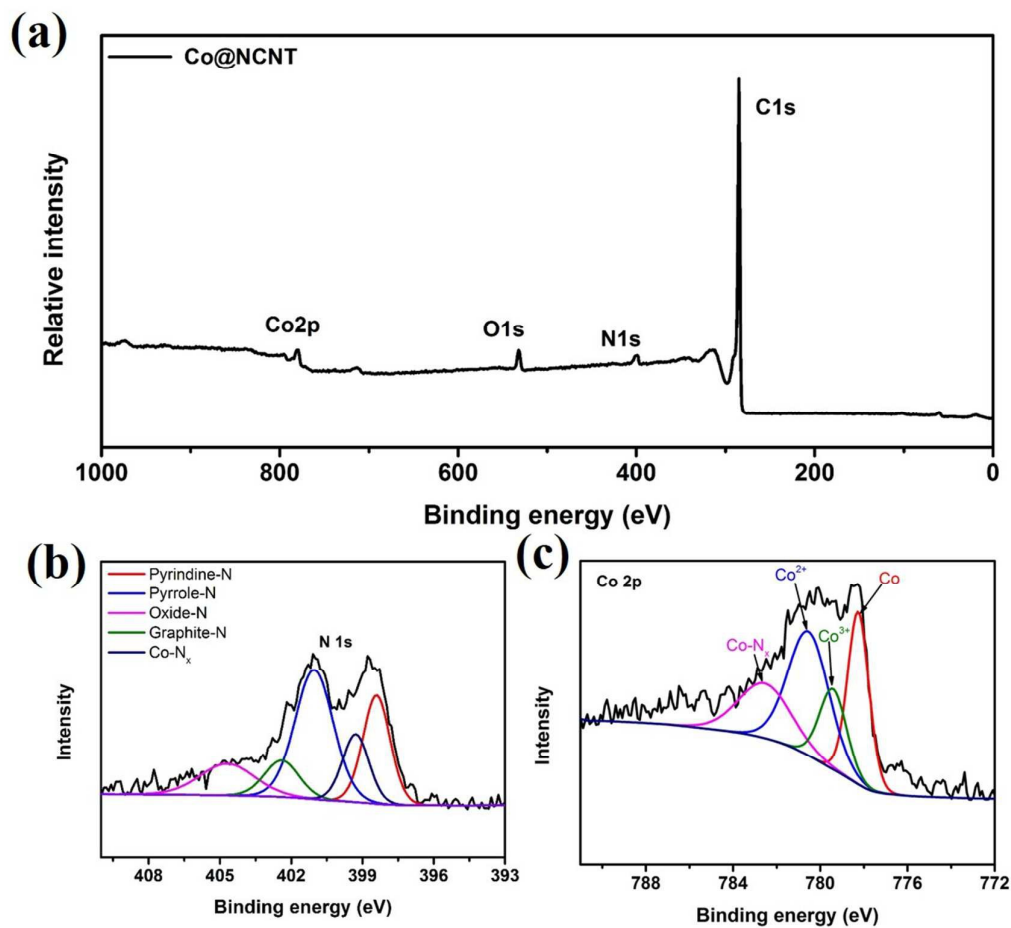


1

2 **Fig. 2.** (a) Powder XRD patterns of sample, (b) N₂ adsorption isotherm and (inset) the
3 corresponding pore size distribution of Co@NCNT.

4

5

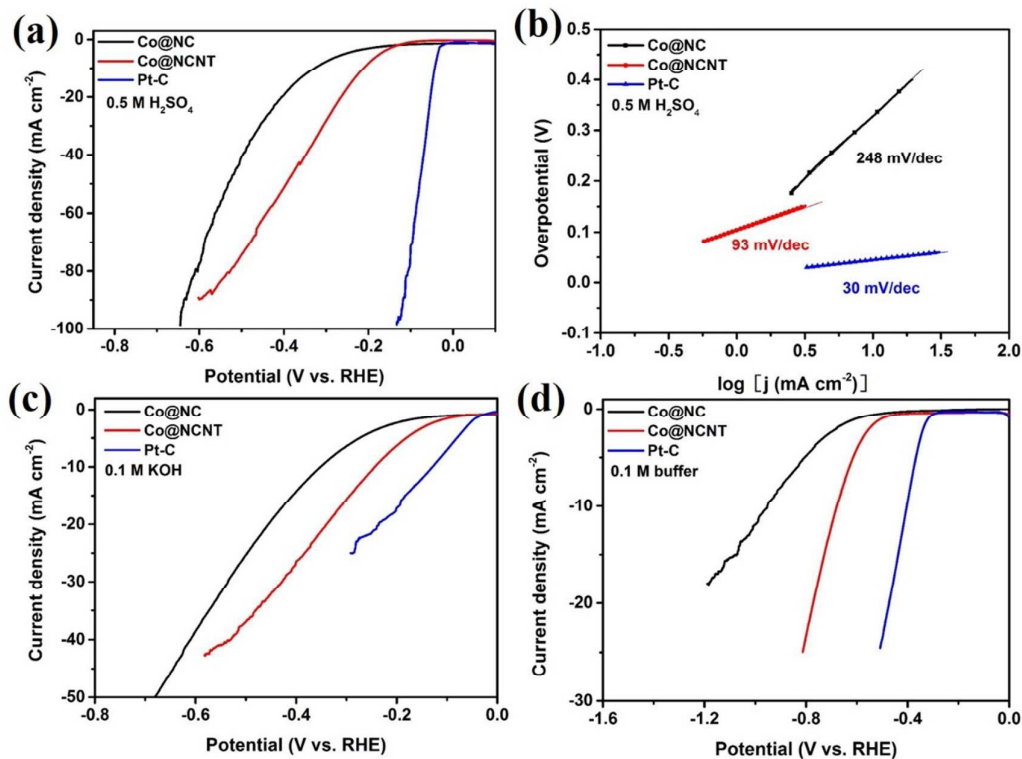


1

2 **Fig. 3.** (a) Survey XPS spectrum, high resolution of (b) N 1s spectrum and (c) Co 2p
3 spectrum for Co@NCNT sample.

4

5

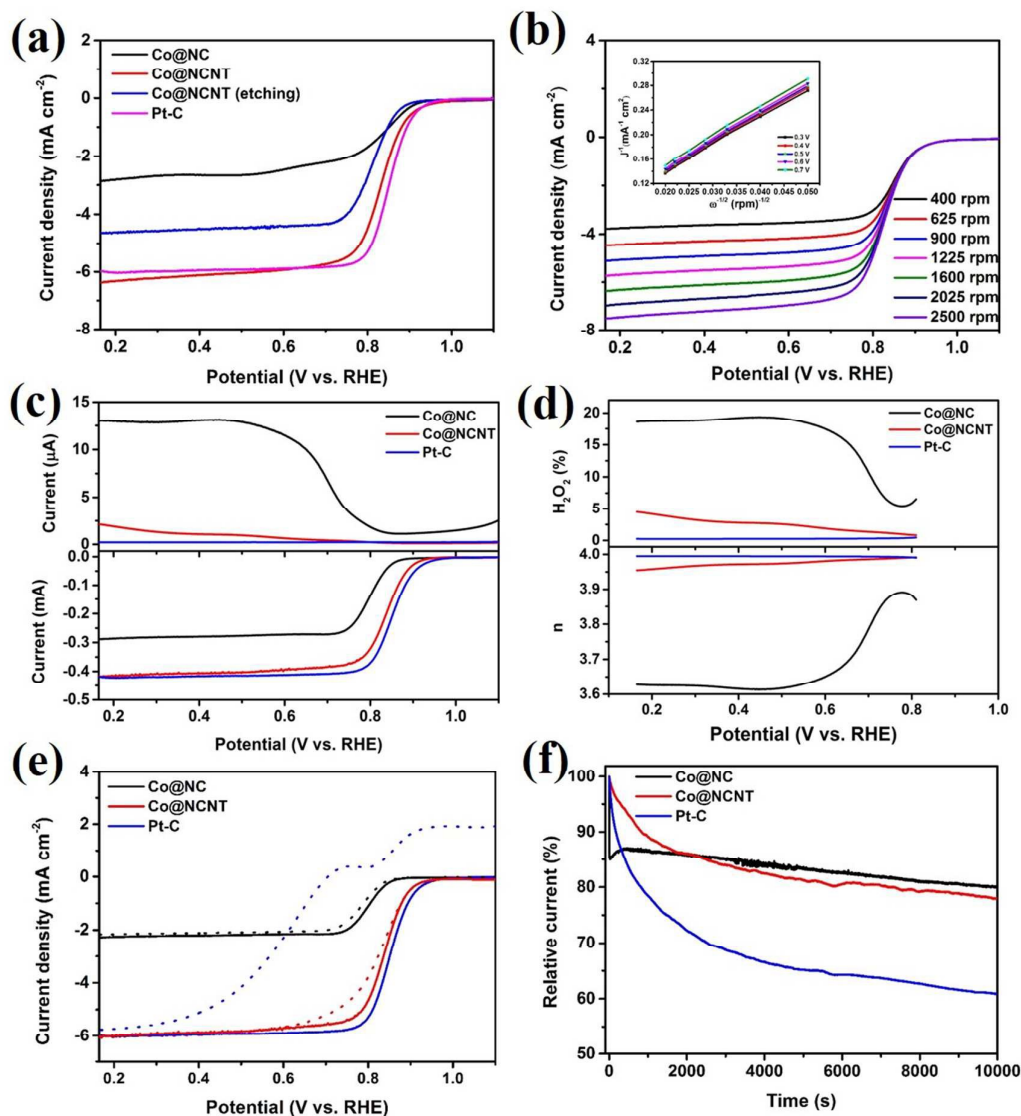


1

2 **Fig. 4.** (a) Linear sweep voltammetry (LSV) curves in 0.5 M H₂SO₄ (pH = 0), (b) The
 3 corresponding Tafel plots in H₂SO₄ solution, and LSV curves in (c) 0.1 M KOH (pH
 4 = 13) and (d) Phosphate buffer (pH = 7) solutions. The active materials modified
 5 electrode at mass loading of 0.425 mg cm⁻², along with Pt/C for comparison.

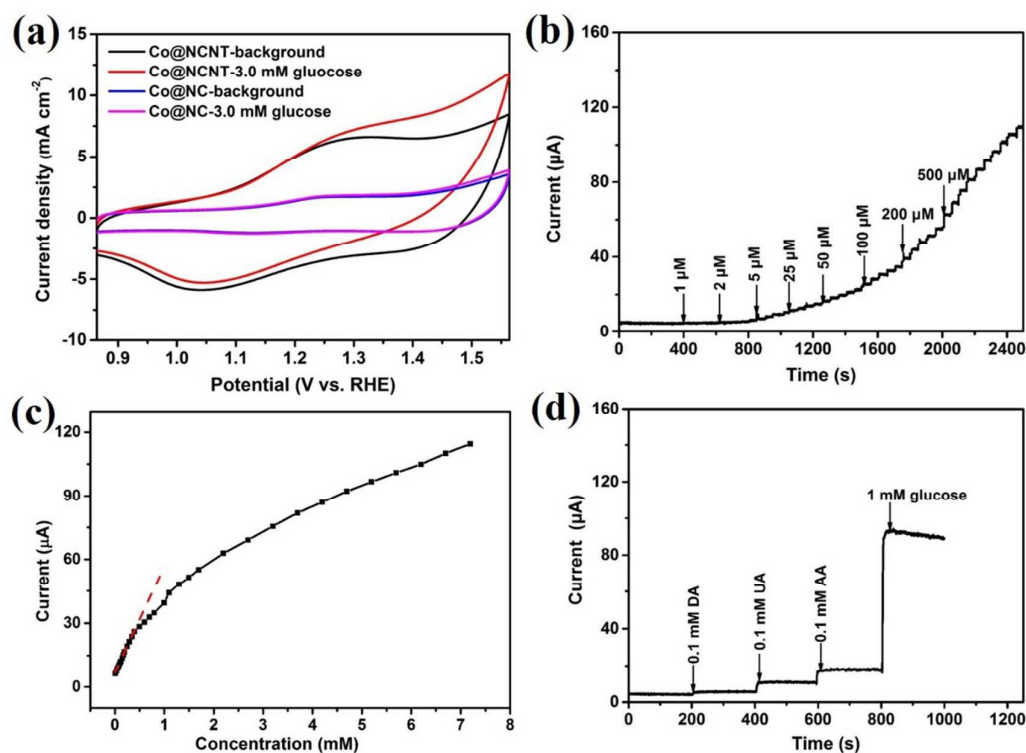
6

7



1
2 **Fig. 5.** (a) RDE polarization curves of Co@NC, Co@NCNT, Co@NCNT after
3 etching and Pt/C in O₂-saturated 0.1 M KOH with a sweep rate of 5 mV s⁻¹ and
4 rotation rate of 1600 rpm, (b) LSV curves of Co@NCNT at various speeds (inset: K-L
5 plots for Co@NCNT at various potentials), (c) RRDE voltammograms recorded with
6 the Co@NC, Co@NCNT and the commercial Pt/C in O₂-saturated 0.1M KOH at
7 1600 rpm, (d) Percentage of peroxide and the electron transfer number (n) of Co@NC,
8 Co@NCNT and the commercial Pt/C at various potentials during ORR, (e) the CVs
9 of the Co@NC, Co@NCNT and the commercial Pt/C electrode in O₂-saturated 0.1 M
10 KOH without (solid line) and with (dotted line) 3 M MeOH, (f) Chronoamperometric

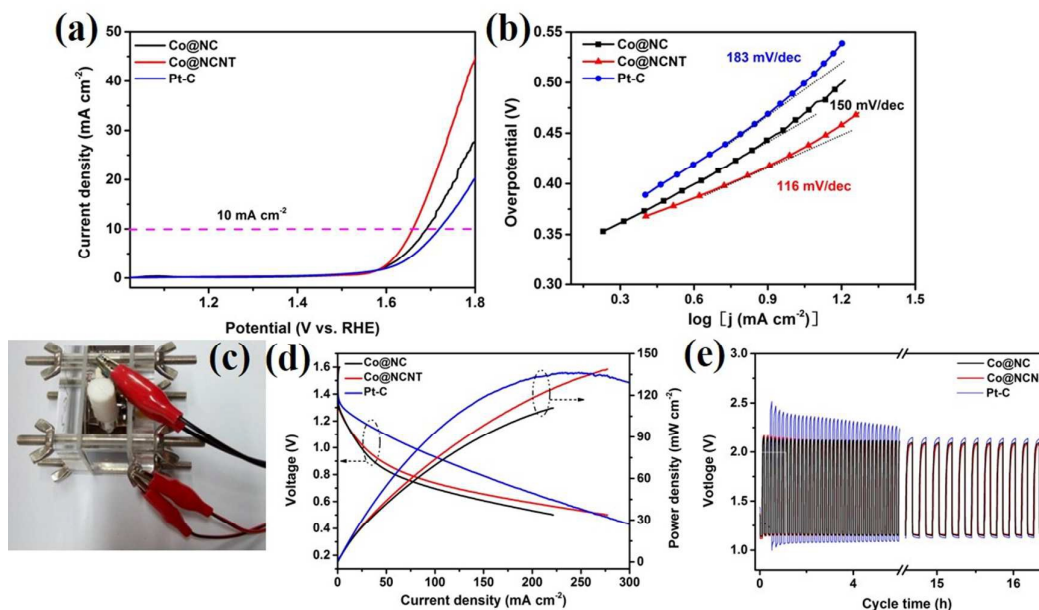
- 1 responses of Co@NC, Co@NCNT and the commercial Pt/C at a constant voltage of
- 2 0.8 V in O₂-saturated 0.1 M KOH solution (1600 rpm).



- 3
- 4 **Fig. 6.** (a) CVs of Co@NCNT and Co@NC electrodes in the absence and presence of
- 5 3.0 mM glucose, respectively, (b) Typical amperometric response of Co@NCNT at
- 6 1.364 V to successive addition of glucose in 0.1 M KOH, (c) Current response vs.
- 7 glucose concentration, (d) Amperometric response of Co@NCNT to the successive
- 8 addition of 0.1 mM DA, 0.1 mM AA, 0.1 mM UA, 1 mM glucose.

9

10



1
2 **Fig. 7.** (a) Polarization curves and (b) corresponding Tafel plots of Co@NCNT,
3 Co@NC and commercial Pt/C catalysts in 1.0 M KOH solution, (c) The optical
4 picture of two-electrode rechargeable zinc-air battery, (d) Discharge polarization
5 curves and corresponding power density curves of primary zinc-air batteries using
6 Co@NCNT, Co@NC, Pt/C as air catalyst (mass loading of 1 mg cm^{-2}), (e) Cycling
7 performance of rechargeable zinc-air batteries with Co@NCNT, Co@NC, Pt/C as the
8 air catalyst at 10 mA cm^{-2} .

9

Graphical Abstract

The hybrid with cobalt nanoparticles embedded in N-rich carbon nanotube (Co@NCNT) has been successfully constructed via pyrolysis of mixture of Co-based metal-organic framework (ZIF-67); the as-developed Co@NCNT exhibits high activity and excellent durability for some important electrochemical reactions, including hydrogen evolution reaction (HER) in pH-universal electrolyte, oxygen reduction reaction (ORR) under both acidic and alkaline media, glucose oxidation reaction (GOR), and oxygen evolution reaction (OER).

